International Journal of Machine Tools & Manufacture 121 (2017) 96–100

Contents lists available at ScienceDirect

International Journal of Machine Tools & Manufacture

journal homepage: www.elsevier.com/locate/ijmactool

Compensation of frequency response function measurements by inverse RCSA

Kadir Kiran, Harsha Satyanarayana, Tony Schmitz*

University of North Carolina at Charlotte, Department of Mechanical Engineering and Engineering Science, Charlotte, NC, USA

ARTICLE INFO

Keywords:
Receptance
Frequency response function
Mass loading
Accelerometer

ABSTRACT

This paper describes an analytical approach for compensating accelerometer-based (contact-type) modal testing results for both mass loading and cable energy dissipation (damping). The inverse Receptance Coupling Substructure Analysis (RCSA) approach is implemented, where a lumped parameter model of the accelerometer-cable is decoupled from the measured receptance (or frequency response function) to isolate the structure's receptance. Experimental results are presented for a 12.7 mm diameter cantilever rod, a 6.35 mm diameter cantilever rod, and clamped-clamped-clamped-free boundary condition thin ribs.

1. Introduction

Machining operations can be stable or unstable depending on the cutting parameters and tool-holder-spindle-machine frequency response function (FRF). In some cases, the workpiece FRF can influence the machining behavior as well. Stable, or chatter-free, cutting conditions can be predicted using process stability models [1–3]. These models require the tool-holder-spindle-machine FRF (and sometimes the workpiece FRF). System FRFs can be obtained by measurement (i.e., modal testing) or models (analytical and/or numerical methods). For the latter, Schmitz and Donaldson [4] first presented the Receptance Coupling Substructure Analysis (RCSA) method to predict tool-holder-spindle-machine FRFs by coupling individual component FRFs (or receptances). This method reduces measurement time because assembly FRFs can be predicted rather than measured. Subsequent efforts by the authors have improved the technique [5–14].

In this paper, a novel application of RCSA is presented in order to improve FRF measurement accuracy. In impact testing, FRFs are measured using an instrumented hammer to excite the system and (typically) an accelerometer to record the response. However, the measured FRF differs slightly from the actual FRF due to the accelerometer and cable mass and cable damping effects. Mass loading compensation has been previously studied in [15–17]. To build on these prior efforts and compensate for both mass loading and cable damping, the inverse RCSA approach is applied here. In this approach, a model of the accelerometer-cable is decoupled from the measured FRF to isolate the structure's FRF. Experimental results are presented for three setups: 1) 12.7 mm diameter cantilever rod; 2) 6.35 mm diameter cantilever rod; and 3) clamped-clamped-clamped-free boundary condition thin ribs.

2. RCSA background

RCSA is used to predict an assembly's receptances by coupling receptances from the individual components. The connections between components can be rigid or flexible with or without energy dissipation (damping) [18]. An example for rigid coupling of two components is displayed in Fig. 1.

For this example, the component direct receptances can be described as $h_{1a1a} = \frac{x_{1a}}{f_{1a}}$ (component I) and $h_{1b1b} = \frac{x_{1b}}{f_{1b}}$ (component II). The compatibility condition for the rigid coupling is $x_{1b} - x_{1a} = 0$. The equilibrium condition, $f_{1a} + f_{1b} = F_1$, relates the internal (component, lower case variable) forces to the external (assembly, upper case variable) forces. The assembly (III) direct receptance, H_{11}, at assembly coordinate X_1 can be expressed as shown in Eq. (1).

$$H_{11} = \frac{X_1}{F_1} = h_{1a1a} - h_{1a1a}(h_{1a1a} + h_{1b1b})^{-1} h_{1a1a} \tag{1}$$

3. Inverse RCSA approach for mass loading compensation

A tool point FRF may be measured by impact testing as shown in Fig. 2a. The experimental FRF differs, at some level, from the actual FRF due to the accelerometer and cable mass for this contact-type measurement. A reduction in the natural frequency(s) and FRF magnitude may be observed, depending on the amount of mass loading and its ratio to the modal mass(es) for the system under test.

The accelerometer-cable mass can be compensated using inverse RCSA, where the corresponding RCSA model is depicted in Fig. 2b. In this model, it is assumed that accelerometer is rigidly coupled to the

* Corresponding author.
E-mail address: tony.schmitz@uncc.edu (T. Schmitz).

http://dx.doi.org/10.1016/j.ijmachtools.2017.04.004
Received 23 September 2016; Received in revised form 25 January 2017; Accepted 4 April 2017
Available online 08 April 2017

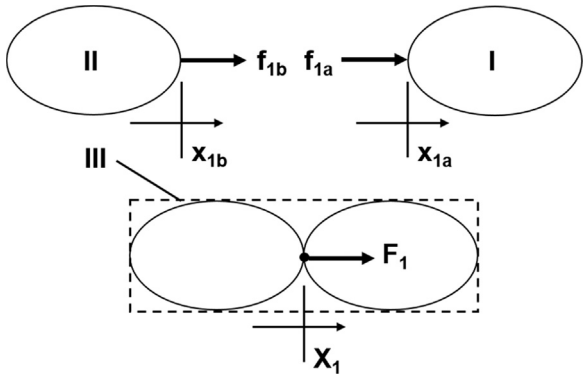

Fig. 1. Two component RCSA model: I and II are individual components and III is the assembly. Component coordinates and forces are lower case; assembly coordinates and forces are upper case.

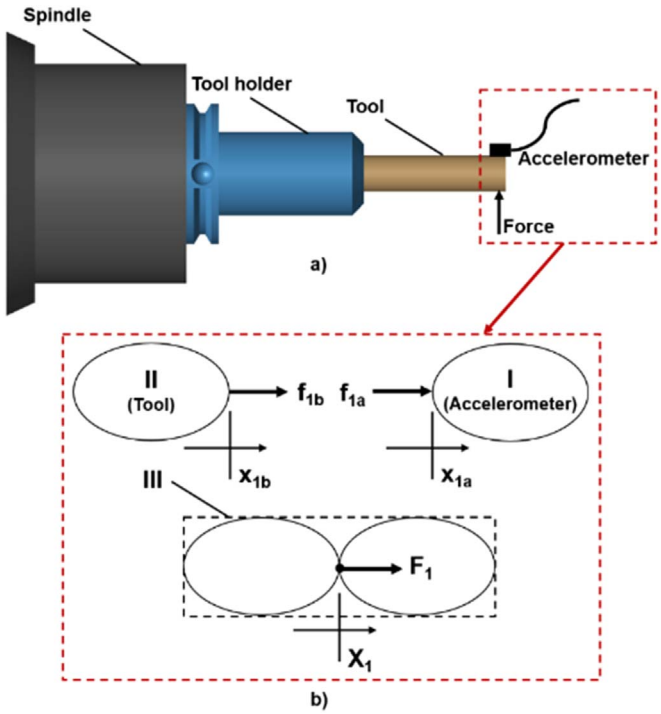

Fig. 2. a) FRF measurement and b) RCSA model.

tool point (using modal wax or other connection strategy). The measurement provides the assembly receptance, $H_{11} = \frac{X_1}{F_1}$. The accelerometer-cable receptance is $h_{1a1a} = \frac{x_{1a}}{f_{1a}}$, while the unknown tool point receptance is $h_{1b1b} = \frac{x_{1b}}{f_{1b}}$. The tool point receptance can be determined by rearranging Eq. (1) as shown in Eq. (2). This approach is referred to as inverse RCSA since Eq. (2) represents a decoupling, rather than a coupling, operation.

$$h_{1b1b} = -h_{1a1a} + h_{1a1a}(h_{1a1a} - H_{11})^{-1} h_{1a1a} \tag{2}$$

For mass compensation only (i.e., mass loading of the structure under test by the accelerometer-cable), the accelerometer-cable may be defined as a point mass. The corresponding receptance (m/N) is provided in Eq. (3), where m is the mass (kg) and ω is the frequency (rad/s).

$$h_{1a1a} = \frac{1}{-m\omega^2} \tag{3}$$

4. Results for mass loading compensation

Experiments were performed on two setups: 12.7 mm diameter and 6.35 mm diameter steel rods with clamped-free boundary conditions. Fig. 3 displays a photograph of the 12.7 mm diameter rod measurement platform. A split clamp was used to hold the rod at the desired cantilever length. The 6.35 mm diameter rod was clamped in an ER16 collet holder with a CAT-40 interface, which was then secured using a manual draw bolt in a spindle nose attached to a large steel block; see Fig. 4.

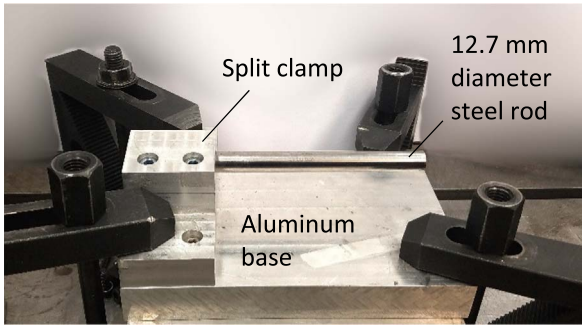

Fig. 3. 12.7 mm diameter rod setup.

For both rod diameters, multiple stickout lengths were selected and measurements were performed with: a medium-size accelerometer (PCB 352A21), a small-size accelerometer (PCB 352C23), and a laser vibrometer (Polytec OFV-534). The latter provided a non-contact measurement reference with no mass loading. To obtain the accelerometer-cable masses, measurements were performed using an Ohaus AV264C Adventurer ProAnalytical Balance (0.1 mg resolution). A measurement example is displayed in Fig. 5, where the accelerometer, the approximate catenary length of the cable from the FRF measurement (to incorporate the cable mass), and the modal wax were included.

Fig. 6 shows the medium accelerometer attachment for a stickout length of 102 mm for the 12.7 mm diameter rod. The measurement and compensation results are displayed in Fig. 7, where the accelerometer-cable mass was 706 mg. It is seen that the accelerometer FRF has a lower natural frequency than the vibrometer (non-contact) FRF. Using Eq. (2) and the measured mass, the mass-loaded FRF was compensated to remove the mass loading effect. This result matches closely with the vibrometer result (the phase error in the vibrometer measurement due to a small time delay between the hammer and vibrometer amplifying electronics was compensated using the technique described in [19]). A summary of the 12.7 mm diameter rod measurement results for both accelerometers at four different stickout lengths is provided in Table 1. The average percent error in the compensated result for all tests is 0.005%. Prior to compensation, the percent error in natural frequency for the medium accelerometer was 1.0% and 0.4% for the small accelerometer.

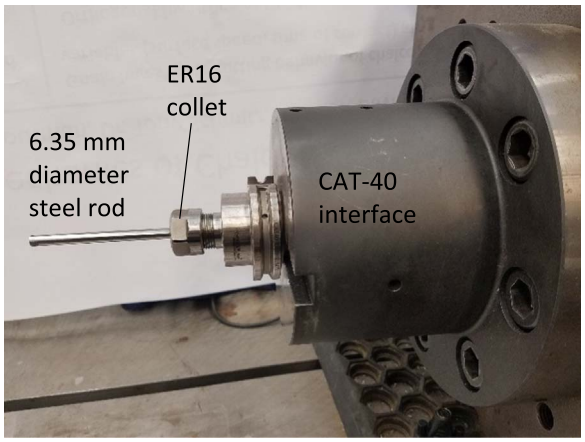

Fig. 4. 6.35 mm diameter rod setup.

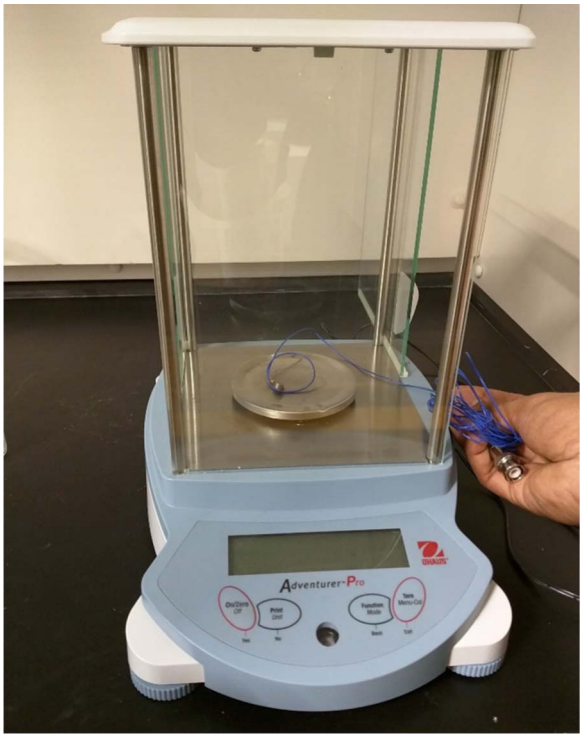

Fig. 5. Accelerometer-cable mass measurement.

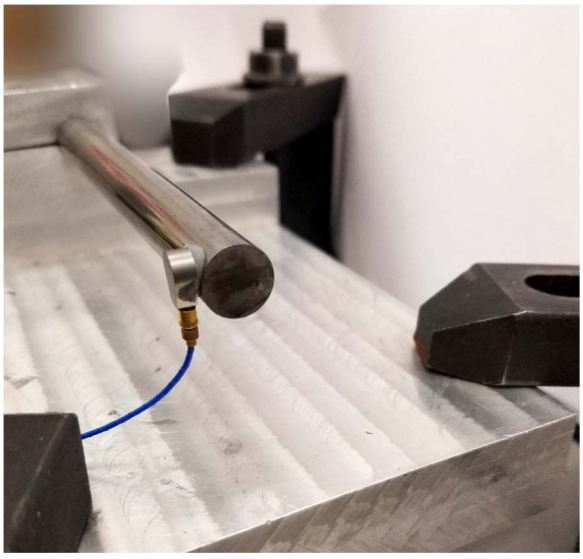

Fig. 6. Medium accelerometer attached to the 12.7 mm diameter rod using modal wax.

Fig. 8 shows the small accelerometer attached to the 6.35 mm diameter rod. Measurement results are presented in Table 2. The average percent error in the compensated results for all tests is −0.09%. Prior to compensation, the percent error in natural frequency for the medium accelerometer was 5.8% and 2.4% for the small accelerometer.

5. Inverse RCSA approach for mass loading and damping compensation

In addition to mass loading, compensation for energy dissipation by the cable may also be included in the inverse RCSA model. In this case, the accelerometer-cable may be defined as a point mass with a lumped parameter (massless) viscous damper. The corresponding receptance (m/N) is provided in Eq. (4), where m is the mass (kg), c is the viscous damping coefficient (N-s/m), and ω is the frequency (rad/s). Alternate modeling approaches, such as structural damping, may also be considered.

$$h_{1a1a} = \frac{1}{-m\omega^2 + i\omega c} \tag{4}$$

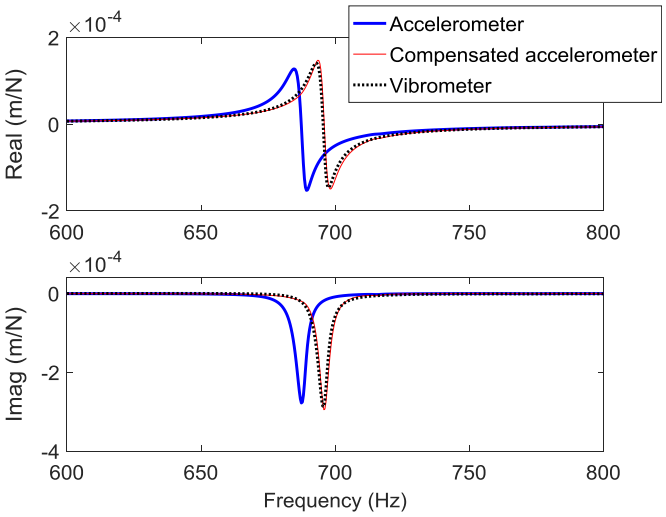

Fig. 7. Results for 12.7 mm diameter rod with a stickout length of 102 mm using the medium accelerometer.

Table 1
12.7 mm diameter rod mass compensation results.

Stick-out (mm)	Vibrometer natl. freq. (Hz)	Accelerometer natl. freq. (Hz)	% error	Compensated natl. freq. (Hz)	% error
Medium accelerometer (706 mg)					
102	695.4	687.4	1.10	695.8	−0.05
111	597.8	592	0.97	598.5	−0.11
118	538.3	533.3	0.92	537.5	0.15
124	492.1	487.1	1.01	492.1	0
Small accelerometer (275 mg)					
102	698.1	695	0.44	698.1	0
111	613.8	611.5	0.37	614.2	−0.06
118	555.4	552.8	0.46	555	0.07
124	503	501.3	0.33	502.8	0.03

*Stickout lengths are approximate. Different setups were used between the small and medium accelerometers.

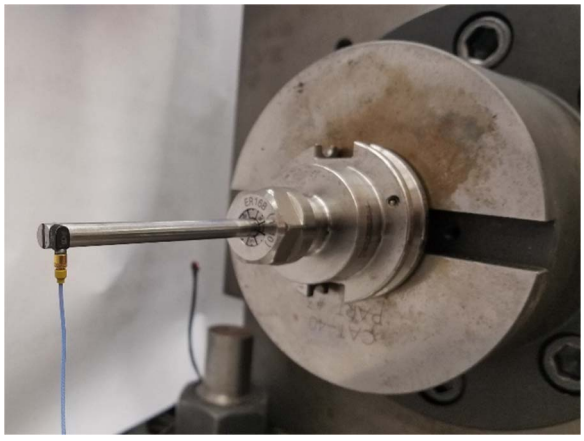

Fig. 8. Small accelerometer attached to the 6.35 mm diameter rod using modal wax.

Table 2
6.35 mm diameter rod mass compensation results.

Stick-out (mm)	Vibrometer natl. freq. (Hz)	Accelerometer natl. freq. (Hz)	% error	Compensated natl. freq. (Hz)	% error
Medium accelerometer (680 mg)					
79	688.2	646.0	6.1	688.9	−0.10
89	546.3	516.0	5.5	547.0	−0.13
Small accelerometer (275 mg)					
79	687.8	671.0	2.4	688.2	−0.06
89	545.5	532.2	2.4	545.9	−0.07

*Stickout lengths are approximate. Different setups were used between the small and medium accelerometers.

6. Results for mass loading and damping compensation

In addition to the 6.35 mm diameter rod measurements, experiments were also performed on two clamped-clamped-clamped-free boundary condition thin ribs. The 6.35 mm diameter rod and ribs represent examples of flexible structures that may have both their FRF natural frequency(s) and amplitudes affected by the contact measurement approach. For the ribs, one rib material was 6061-T6 aluminum and the other was 6Al-4V titanium. The titanium rib was approximately an order of magnitude stiffer than the aluminum rib at the center of the unsupported edge. The small accelerometer and laser vibrometer were used for the rib measurements. The setup is shown in Fig. 9, where the thin ribs were fixed to the table using cyanoacrylate and the measurement location was the center of the unsupported edge.

Figs. 10–12 display measurement and compensation results. In Fig. 10, FRFs for the 6.35 mm diameter rod with a stickout length of 89 mm are displayed. It is seen that the accelerometer-based FRF has a lower natural frequency (due to the mass loading) and a reduced amplitude (due to the cable damping). The measured accelerometer-cable mass was substituted in Eq. (4) and the damping coefficient was adjusted to provide an amplitude match between the compensated FRF and vibrometer FRF. The aluminum and titanium rib results are shown in Figs. 11 and 12. The mass loading and damping compensation results for the 6.35 mm diameter rod and both ribs are summarized in Table 3.

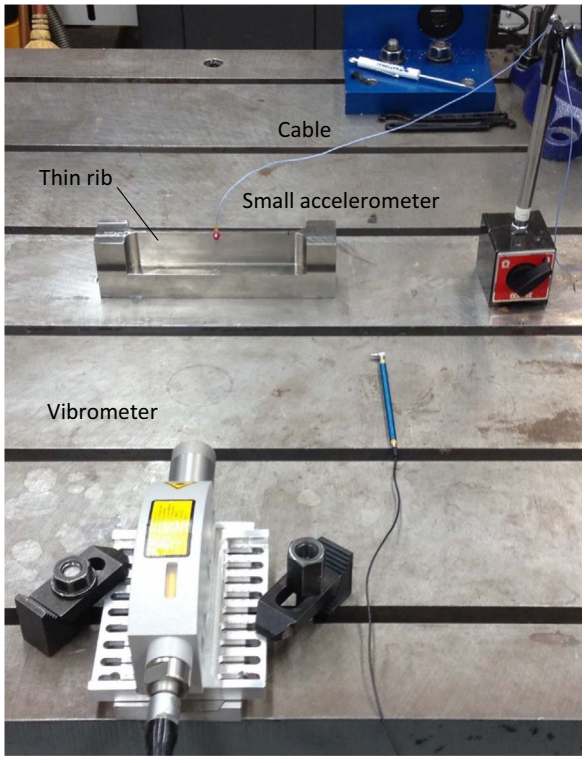

Fig. 9. Thin rib setup.

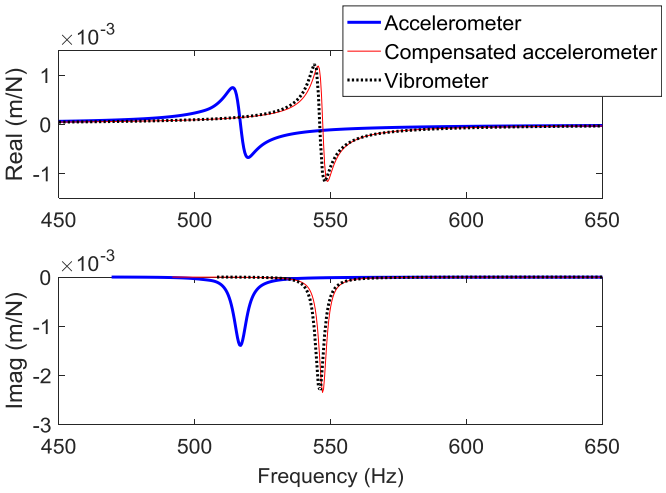

Fig. 10. 6.35 mm diameter rod results for medium accelerometer with 89 mm stickout length.

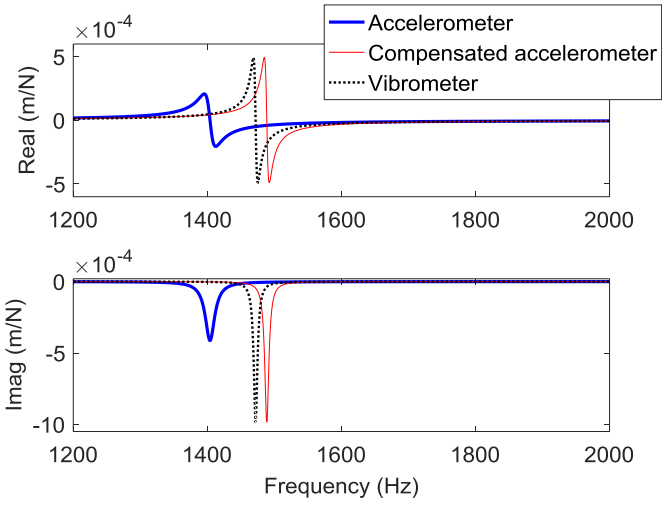

Fig. 11. Aluminum rib results.

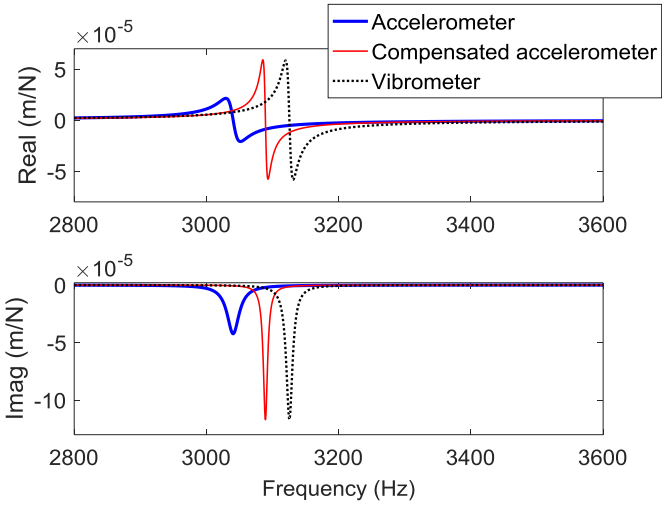

Fig. 12. Titanium rib results.

Although this does not represent a comprehensive study of cable

Table 3
Mass loading and damping compensation results.

Structure	Vibrometer natl. freq. (Hz)	Accelerometer natl. freq. (Hz)	% error	Compensated natl. freq. (Hz)	% error	c (N-s/m)
6.35 mm rod	Medium accelerometer (680 mg)					
79 mm	688.2	646.0	6.1	688.9	−0.10	0.13
89 mm	546.3	516.9	5.4	547.0	−0.13	0.15
6.35 mm rod	Small accelerometer (275 mg)					
79 mm	687.8	671.0	2.4	688.2	−0.06	0.07
89 mm	545.5	532.2	2.4	545.9	−0.07	0.07
Rib	Small accelerometer (286.4 mg)					
Al 6061-T6	1472.0	1404.0	4.6	1488.7	−1.13	0.17
Ti 6Al-4V	3125.5	3040.4	2.7	3089.2	1.16	0.85

damping effects, conclusions can be drawn from Table 3. First, for a single structure and a single accelerometer, the damping value was consistent. Specifically, 1) c=0.07 N-s/m for both 6.35 mm diameter rod measurements using the small accelerometer; and 2) c=0.13 N-s/m and 0.15 N-s/m for the 6.35 mm diameter rod measurements using the medium accelerometer. Presumably, the change is c values is due to the difference in cables and/or cable configuration between the two accelerometers/setups. Second, the c value may scale with the structure's stiffness. Of the three structures, the 6.35 mm diameter rod was the most flexible, followed by the aluminum rib, and, finally, the titanium rib. Considering the small accelerometer, the c values increase from 0.07 to 0.17 to 0.85, respectively, for these three setups. Future testing will focus on an improved understanding of the viscous damping coefficient required to compensate for cable-based energy dissipation.

7. Conclusions

This paper described the application of inverse Receptance Coupling Substructure Analysis (RCSA) to mass and damping compensation for accelerometer-based impact testing. The measurement (assembly) FRF was used together with a point mass-viscous damping model of the accelerometer-cable to determine the compensated tool point FRF using the analytical inverse RCSA approach. Experiments were completed for: 1) two rod diameters and multiple stickout lengths for clamped-free rod boundary conditions; and 2) thin ribs with clamped-clamped-clamped-free boundary conditions. The average percent error in compensated natural frequency over all 14 tests reported in this study was −0.02%.

A limitation to the compensation procedure is that a first-principles approach to predict the viscous damping coefficient based on cable properties is not presented. However, the absence of physics-based models is true, in general, for mechanical damping in structures. Consider finite element analysis, for example. The eigensolution (natural frequencies and mode shapes) can be predicted quite accurately if boundary conditions are properly described. However, if scaled FRFs are desired, the damping type and values must be entered based on the user's prior experience. The approach presented here provides a mechanism for incorporating damping, as well as mass, in FRF compensation and motivates future work to approximate, tabulate, and (potentially) model the cable behavior.

Acknowledgements

This material is based upon work supported by the National Science Foundation under Grant No. CMMI-1561221.

References

[1] G. Tlusty, Manufacturing Processes and Equipment, Prentice Hall, Upper Saddle River, NJ, 2000.
[2] Y. Altintas, Manufacturing Automation: Metal Cutting Mechanics, Machine Tool Vibrations, and CNC Design, Cambridge University Press, Cambridge, UK, 2000.
[3] T.L. Schmitz, K.S. Smith, Machining Dynamics: Frequency Response to Improved Productivity, Springer, New York, NY, 2009.
[4] T.L. Schmitz, R.R. Donaldson, Predicting high-speed machining dynamics by substructure analysis, CIRP Ann.-Manuf. Technol. 49/1 (2000) 303–308.
[5] T. Schmitz, M. Davies, K. Medicus, J. Snyder, Improving high-speed machining material removal rates by rapid dynamic analysis, Ann. CIRP 50/1 (2001) 263–268.
[6] T. Schmitz, M. Davies, M. Kennedy, Tool point frequency response prediction for high-speed machining by RCSA, J. Manuf. Sci. Eng. 123 (2001) 700–707.
[7] G.S. Duncan, M. Tummond, T. Schmitz, An investigation of the dynamic absorber effect in high-speed machining, Int. J. Mach. Tools Manuf. 45 (2005) 497–507.
[8] T. Schmitz, G.S. Duncan, Three-component receptance coupling substructure analysis for tool point dynamics prediction, J. Manuf. Sci. Eng. 127/4 (2005) 781–790.
[9] T. Schmitz, G.S. Duncan, Receptance coupling for dynamics prediction of assemblies with coincident neutral axes, J. Sound Vib. 289/4–5 (2006) 1045–1065.
[10] T. Schmitz, K. Powell, D. Won, G.S. Duncan, W.G. Sawyer, J. Ziegert, Shrink fit tool holder connection stiffness/damping modeling for frequency response prediction in milling, Int. J. Mach. Tools Manuf. 47/9 (2007) 1368–1380.
[11] C.-H. Cheng, G.S. Duncan, T. Schmitz, Rotating tool point frequency response prediction using RCSA, Mach. Sci. Technol. 11/3 (2007) 433–446.
[12] S. Filiz, C.-H. Cheng, K. Powell, T. Schmitz, O. Ozdoganlar, An improved tool-holder model for RCSA tool-point frequency response prediction, Precis. Eng. 33 (2009) 26–36.
[13] T. Schmitz, Torsional and axial frequency response prediction by RCSA, Precis. Eng. 34 (2010) 345–356.
[14] U. Kumar, T. Schmitz, Spindle dynamics identification for receptance coupling substructure analysis, Precis. Eng. 36/3 (2012) 435–443.
[15] D.J. Ewins, Modal Testing: Theory, Practice and Application, 2nd ed., Wiley, New York, NY, 2009.
[16] O. Özşahin, H.N. Özgüven, E. Budak, Analysis and compensation of mass loading effect of accelerometers on tool point FRF measurements for chatter stability predictions, Int. J. Mach. Tools Manuf. 50/6 (2010) 585–589.
[17] D. Olvera, A. Elías-Zúñiga, O. Martínez-Romero, L.L. de Lacalle, H. Martínez-Alfaro, H.R. Siller, M.W. Pineda, Improved predictions of the stability lobes for milling cutting operations of thin-wall components by considering ultra-miniature accelerometer mass effects, Int. J. Adv. Manuf. Technol. 86/5–8 (2016) 2139–2146.
[18] T.L. Schmitz, K.S. Smith, Mechanical Vibrations: Modeling and Measurement, Springer, New York, NY, 2012.
[19] V. Ganguly, T.L. Schmitz, Phase correction for frequency response function measurements, Precis. Eng. 38 (2014) 409–413.